Distinguishing between dark-matter interactions with gravitational-wave detectors

Andrew L. Miller,[1,*] Francesca Badaracco,[1,†] and Cristiano Palomba[2,‡]
[1]*Université catholique de Louvain, B-1348 Louvain-la-Neuve, Belgium*
[2]*INFN, Sezione di Roma, I-00185 Roma, Italy*

(Received 7 April 2022; accepted 20 May 2022; published 31 May 2022)

Ground-based gravitational-wave interferometers could directly probe the existence of ultralight dark matter [$\mathcal{O}(10^{-14}$–$10^{-11})$ eV$/c^2$] that couples to standard model particles in the detectors. Recently, many techniques have been developed to extract a variety of potential dark-matter signals from noisy gravitational-wave data; however, little effort has gone into ways to distinguish between types of dark matter that could directly interact with the interferometers. In this work, we employ the Wiener filter to follow-up candidate dark-matter interaction signals. The filter captures the stochastic nature of these signals and, in simulations, successfully identifies which type of dark matter interacts with the interferometers. The power of this method to distinguish between different types of dark matter comes from different coupling mechanisms that result in different power spectra, as well as different correlations between detectors spread across the Earth. We apply the Wiener filter to outliers that remained in the LIGO/Virgo/KAGRA search for dark photons in data from the most recent observing (O3) [R. Abbott *et al.* (LIGO Scientific, Virgo, KAGRA Collaborations), Phys. Rev. D **105**, 063030 (2022)] and show that they are consistent with noise disturbances. Our proof-of-concept analysis demonstrates that the Wiener filter can be a powerful technique to confirm or deny the presence of dark-matter interaction signals in gravitational-wave data and distinguish between scalar and vector dark-matter interactions.

DOI: 10.1103/PhysRevD.105.103035

I. INTRODUCTION

The existence of dark matter has puzzled scientists for the last few decades. While ample evidence supports an invisible type of matter that moves the stars in our Galaxy around faster than we would expect based on visible matter [1], that gravitationally lenses light in the Bullet cluster [2] and that explains anisotropies in the cosmic microwave background power spectrum [3], the underlying nature of dark matter has eluded our understanding. Theories of beyond standard model physics allow dark matter to have a mass as light as $\sim 10^{-22}$ eV$/c^2$ or as heavy as ~ 1 PeV$/c^2$ [4]. Additionally, dark matter could be macroscopic and composed in part or completely of primordial black holes [5]. To search for dark matter in such a wide parameter space, different experiments have been designed, some that probe dark matter via its direct interaction (scattering) with standard model particles [6–8] and others that look for dark matter indirectly via electromagnetic signatures resulting from the annihilation or decay of dark-matter particles [9].

Though not constructed for the specific reason to detect dark matter, gravitational-wave interferometers, such as LIGO [10], Virgo [11], and KAGRA [12], offer an innovative and competitive way to search for ultralight dark matter in the mass range $\mathcal{O}(10^{-14}$–$10^{-11})$ eV$/c^2$. These detectors rely on high-precision measurements of the positions of the mirrors in each arm of the laser interferometer that would follow a path in spacetime carved out by a passing gravitational wave [13]. In our work, though, we do not look for a signature of gravitational waves, but for one of a direct interaction of dark-matter particles with components of the gravitational-wave interferometers. Thus, LIGO, Virgo, and KAGRA become similar to particle physics, direct-detection experiments.

Recently, searches for different types of scalar and vector ultralight dark matter have been performed. The analysis of GEO600 data [14] using a logarithmic frequency axis power spectral density method [15,16] yielded competitive constraints on scalar, dilaton dark matter [17–20] that could have coupled to electrons and photons in the beam splitter [21]. Furthermore, constraints on vector dark matter, i.e., dark photons, were placed using data from the first [22] and third [23] observing runs of advanced LIGO/Virgo that surpassed upper limits from the Eöt-Wash [24] and MICROSCOPE [25] experiments by a few orders of magnitude at frequencies between $\sim$100–1000 Hz ($4 \times 10^{-13} - 4 \times 10^{-12}$ eV$/c^2$). The existence of ultralight dark matter has also been constrained by searching for

*andrew.miller@uclouvain.be
†francesca.badaracco@uclouvain.be
‡cristiano.palomba@roma1.infn.it

gravitational waves from depleting boson clouds around black holes [26–32] and by analyzing mergers, e.g., GW190521 [33], which was shown to be consistent with the merger of complex vector boson stars [34].

Though the field of direct dark-matter detection with gravitational-wave interferometers is blossoming, a key question remains unanswered: in the event of a detection, will it be possible to *distinguish* among different ultralight dark-matter interaction models? As explained in the next section, dark matter could be composed of scalar or vector particles that would both leave similar imprints on gravitational-wave interferometers. Current analysis methods based on cross-correlation [35] and excess power [36] allow for the detection of *a* dark-matter particle but cannot determine *which* dark-matter particle has actually been observed because these methods match their analysis coherence times to the coherence time of the ultralight dark-matter signal. This finite coherence time arises because individual particles in the dark-matter wave packet travel with slightly different velocities that follow a Maxwell-Boltzmann distribution centered about the virial velocity v_0 of dark matter: $v_0 = 220$ km/s.[1] In this work, we propose a new method based on the Wiener filter [37] to distinguish among the different types of interactions using their similar but distinct power spectra.

II. DARK-MATTER INTERACTION MODELS

Different types of dark matter would leave different signatures in gravitational-wave interferometers. Regardless of the type of dark matter, certain properties collectively characterize the nature of the signal [38]. First, the occupation number of ultralight dark matter is gigantic, $\mathcal{O}(10^{50})$, which implies that the wave functions of individual dark-matter particles overlap. Second, ultralight dark matter is cold, so the velocities of these dark-matter particles follow a Maxwell-Boltzmann distribution, centered about the virial velocity. Third, dark matter behaves as a classical sinusoidal field within its coherence time, oscillating at a frequency that is proportional to the dark-matter mass. Fourth, when observing for longer than a coherence time, ultralight dark matter will not oscillate at a fixed frequency but rather *about* that frequency, with stochastic frequency variations $\Delta f/f \sim \mathcal{O}(v_0^2/c^2) \sim 10^{-6}$ [35].

In the following subsections, we describe the differences between ultralight scalar and vector dark matter and the specific ways in which these particles would generate a signal in gravitational-wave detectors.

[1]This quantity is the velocity at which dark matter orbits the center of our Galaxy.

A. Scalar dark matter

Models for scalar, spin-0 dark matter have received a lot of attention over the last few decades. Examples of these particles include the QCD axion [39–42], which appears naturally as a pseudo Nambu-Goldstone boson of a spontaneous global $U(1)$ symmetry breaking that also solves the strong charge-parity (CP) problem, and the dilaton, which can occur in multidimensional theories [43–48].

Axions could alter the phase velocities of circularly polarized photons in the laser beams traveling down each arm of the detector [49]. Such a signal would actually be visible in other channels aside from the canonical gravitational-wave one [50] and would require additional but simplistic optical components to measure the optical path difference between p- and s-polarized light. In practice, linearly polarized light (p) is inputted, and the axion causes polarization modulations, producing s-polarized light. Linearly polarized light can be expressed as a superposition of circularly polarized light.

On the other hand, dilatonlike dark matter [17–19] could change the mass of the electron and other physical constants, causing oscillations in the Bohr radius of atoms in various components of the interferometer [20]. In particular, the size and index of refraction of the beam splitter would oscillate over time; thus, light rays returning to the beam splitter from the interferometer cavities would traverse slightly different distances on the surface of the beam splitter, leading to a differential strain.

Such a scalar ultralight dark-matter field ϕ can be written as [21,48,51]

$$\phi(t,\vec{r}) = \left(\frac{\hbar\sqrt{2\rho_{\mathrm{DM}}}}{m_\phi c}\right)\cos(\omega_\phi t - \vec{k}_\phi\cdot\vec{r}), \tag{1}$$

where t is time, $\vec{r}$ is a position vector, $\hbar$ is Planck's reduced constant, c is the speed of light, $\omega_\phi = (m_\phi c^2)/\hbar$ is the angular Compton frequency, $\vec{k}_\phi = (m_\phi \vec{v}_{\mathrm{obs}})/\hbar$ is the wave vector, m_ϕ is the mass of the field, and $\vec{v}_{\mathrm{obs}}$ is the velocity of the dark matter relative to the observer.

The Lagrangian $\mathcal{L}_{\mathrm{int}}$ for this scalar field is [21]

$$\mathcal{L}_{\mathrm{int}} \supset \frac{\phi}{\Lambda_\gamma}\frac{F_{\mu\nu}F^{\mu\nu}}{4} - \frac{\phi}{\Lambda_e}m_e\bar{\psi}_e\psi_e, \tag{2}$$

where $F_{\mu\nu} = \partial_\mu A_\nu - \partial_\nu A_\mu$ is the electromagnetic field tensor, ψ_e and $\bar{\psi}_e$ are the standard-model electron field and its Dirac conjugate, and Λ_γ and Λ_e denote the scalar dark-matter coupling parameters to the photon and electron, respectively.

Such couplings would cause changes in the index of refraction and sizes of materials and would lead to a differential displacement $\delta(L_x - L_y)$ on gravitational-wave interferometers given by [20]

$$\delta(L_x - L_y) \approx \left(\frac{1}{\Lambda_\gamma} + \frac{1}{\Lambda_e}\right)\left(\frac{nl\hbar\sqrt{2\rho_{\rm DM}}}{m_\phi c}\right)\cos(\omega_{\rm obs}t), \quad (3)$$

where n and l are the index of refraction and length of the beam splitter, respectively.

B. Vector dark matter

Dark matter could be composed of spin-1 particles, which we denote as the dark photon. The relic abundance of dark matter can be explained entirely by dark photons, which could arise from the misalignment mechanism [52–54], parametric resonance or the tachyonic instability of a scalar field [55–58] or from cosmic string network decays [59]. Dark photons could couple directly to baryon or baryon-lepton number in the four primary interferometer mirrors that serve as gravitational-wave test masses and exert a "dark" force on the mirrors, causing quasisinusoidal oscillations [35,36].

We formulate dark photons in a way analogous to ordinary photons: as having a vector potential with an associated dark electric field that causes a quasisinusoidal force on the mirrors in the interferometers.

The vector potential for a single dark photon particle can be written as

$$\vec{A} = \left(\frac{\hbar\sqrt{2\rho_{\rm DM}}}{m_A c^2}\frac{1}{\sqrt{\epsilon_0}}\right)\sin(\omega_A t - \vec{k}_A\cdot\vec{r} + \Upsilon), \quad (4)$$

where $\omega_A = (m_A c^2)/\hbar$ is the angular Compton frequency, $\vec{k}_A = (m_A\vec{v}_{\rm obs})/\hbar$ is the wave vector, m_A is the mass of the vector field, ϵ_0 is the permittivity of free space, and Υ is a random phase.

The Lagrangian $\mathcal{L}$ that characterizes the dark photon coupling to a number current density J^μ of baryons or baryons minus leptons is

$$\mathcal{L} = -\frac{1}{4\mu_0}F^{\mu\nu}F_{\mu\nu} + \frac{1}{2\mu_0}\left(\frac{m_A c}{\hbar}\right)^2 A^\mu A_\mu - \epsilon e J^\mu A_\mu, \quad (5)$$

where $F_{\mu\nu}$ now indicates the dark electromagnetic field tensor, μ_0 is the magnetic permeability in vacuum, m_A is the dark photon mass, A_μ is the 4-vector potential of the dark photon, e is the electric charge, and ϵ is the strength of the particle/dark photon coupling normalized by the electromagnetic coupling constant.

Dark photons cause small motions of an interferometer's mirrors and lead to an observable effect in two ways. First, the mirrors are well separated from each other and hence experience slightly different dark photon dark-matter phases. Such a phase difference leads to a differential change of the arm length, suppressed by v_0/c. This effect is, in fact, a residual one: if the mirrors of current gravitational-wave interferometers had different material compositions from each other, then the signal induced from dark photons coupling to baryon-lepton number would be enhanced [60]. A simple relation between dark photon parameters and the effective strain h_D can be written as [35]

$$\sqrt{\langle h_D^2\rangle} = C\frac{q}{M}\frac{v_0}{2\pi c^2}\sqrt{\frac{2\rho_{\rm DM}}{\epsilon_0}}\frac{e\epsilon}{f_0}, \quad (6)$$

where q/M is the charge-to-mass ratio of the mirrors, f_0 is the frequency of the dark-matter particle, and $C = \sqrt{2}/3$ is a geometrical factor obtained by averaging over all possible dark photon propagation and polarization directions. Second, the common motion of the interferometer mirrors, induced by the dark photon dark-matter background, can lead to an observable signal because of the finite travel time of the laser light in the interferometer arms. The light will hit the mirrors at different times during their common motions, and although the common motions do not change the instantaneous arm length, they can lead to a longer round-trip travel time for the light, equivalent to arm lengthening, and therefore an apparent differential strain [61]. Similarly to Eq. (6), the common motion induces an observable signal with an effective strain h_C as

$$\sqrt{\langle h_C^2\rangle} = \frac{\sqrt{3}}{2}\sqrt{\langle h_D^2\rangle}\frac{2\pi f_0 L}{v_0}. \quad (7)$$

The interference between the two contributions to the strain averages to zero over time, which means that the total effective strain can be written as $\langle h_{\rm total}^2\rangle = \langle h_D^2\rangle + \langle h_C^2\rangle$.

III. WIENER FILTERING

The Wiener filter has been applied in the context of gravitational-wave data analysis before, specifically in terms of reducing Newtonian noise [62], detecting a stochastic gravitational-wave background [63], and handling the presence of correlated noise [64–66]. Here, however, we apply the Wiener filter to a new problem: searching for ultralight dark matter.

Coherence times for ultralight dark matter in the mass range considered here range from hours to days, which is much less than the approximately one-year observation time of a ground-based gravitational-wave detector. Thus, standard ultralight dark-matter searches [21–23,35,36] must restrict their analysis coherence times (that is, the fast Fourier transform length $T_{\rm FFT}$) to match that of the ultralight dark-matter coherence time and sum the power in these individual chunks. While these methods ensure that power remains within one frequency bin in each chunk, they mask the stochastic nature of the signal; thus, all ultralight dark-matter interactions with gravitational-wave detectors would appear the same if detected by these methods. Thus, we propose to use Wiener filtering to extract different types of ultralight dark-matter signals from LIGO/Virgo/KAGRA data.

A. Method description

Typically, the Wiener filter can be used to estimate signal parameters in the presence of noise, and its formulation is the basis of least-square error applications (such as linear prediction and adaptive filters). The Wiener filter coefficients are calculated by minimizing the mean squared error between a finite impulse response (FIR) filter [Eq. (8)] and the target signal. The least-square error filter theory assumes that the signals are stationary processes [67]. We can linearly reconstruct a signal from a multiple inputs [multiple-input/single-output (MISO) filter]:

$$\begin{aligned}\hat{x}[m] &= \sum_{k=0}^{P-1} w_{k_0} y_0[m-k] + \cdots + \sum_{k=0}^{P-1} w_{k_N} y_N[m-k] \\ &= \sum_{k=0}^{P-1} \mathbf{w}_k^T \mathbf{y}[m-k]. \end{aligned} \tag{8}$$

Here, $\hat{x}[m]$ is the estimated discrete target signal at time m (the ultralight dark-matter signal in our case), and $y_i[m-k]$ are the N discrete input signals collected from N witness sensors at the time $m-k$ (the gravitational-wave detectors). This is a MISO linear filter of order P, which means that we use P coefficients and P past values of each witness signal, $y_i[m]$; $\mathbf{w}_k$ represents the kth vector of the Wiener filter coefficients, while $\mathbf{y}[m]$ is the vector containing the N signals from all the witness channels. For the purposes of detecting and validating an ultralight dark-matter signal, we do not need to reconstruct it in the time domain; therefore, we can employ the Wiener filter in the frequency domain. In this way, the information regarding the order of the filter disappears. Indeed, Eq. (8) is a discrete convolution of functions with finite support, so we can apply the convolution theorem, which connects the z-transforms of the filter input and output by means of the filter transfer function. For a filter described by Eq. (8), it is always possible to work on the unit circle of the complex plane and express the relation among input and output through the discrete-time Fourier transform [68]. This means that we can apply the Fourier transform to a block of M samples and rewrite Eq. (8) as

$$\hat{X}(\omega) = \mathbf{W}^T(\omega)\mathbf{Y}(\omega) = \mathbf{Y}^T(\omega)\mathbf{W}(\omega), \tag{9}$$

where both $\mathbf{W}(\omega)$ and $\mathbf{Y}(\omega)$ are N-dimensional vectors containing the discrete Fourier transforms of the Wiener filter coefficients and the N witness signals, respectively. The Wiener filter is then defined by the coefficients that minimize the ensemble average of the square error function, $E[e^*[m]e[m]]$, with $e[m] = x[m] - \hat{x}[m]$:

$$E[e^*e] = E[(X - \mathbf{Y}^T\mathbf{W})^*(X - \mathbf{Y}^T\mathbf{W})]. \tag{10}$$

Minimizing $E[e^*[m]e[m]]$ with respect to the Wiener filter coefficients, we obtain its optimal value

$$\mathbf{W} = (\bar{\mathbf{P}}_{YY})^{-1}\mathbf{P}_{XY}, \tag{11}$$

where $\bar{\mathbf{P}}_{YY}$ is the $N \times N$ matrix containing the cross–power spectral densities (PSDs) of the N witness sensors, while $\mathbf{P}_{XY}$ is the vector containing the cross-PSD between the N witness sensors and the target signal model. With this result, we can rewrite $E[e^*e]$ to define the residual as the ensemble average of the least-square error normalized by the target signal PSD ($P_{XX}(\omega) = E[X^*(\omega)X(\omega)]$):

$$R(\omega) = 1 - \frac{\mathbf{P}_{XY}^\dagger \bar{\mathbf{P}}_{YY}^{-1} \mathbf{P}_{XY}}{P_{XX}}. \tag{12}$$

Given the properties of the PSD, $R(\omega)$ will be real valued and constrained between 0 and 1. In the context of this work, $X(\omega)$ represents the template of the ultralight dark-matter signal we will use to determine if the data $Y(\omega)$ contain the ultralight dark-matter signal.

B. Combining multiple detectors

Assuming each detector's signal is the sum between the ultralight dark-matter signal and the detector's self-noise, we can retrieve the self-noise limiting curve of the Wiener filter. We consider the ideal case in which correlations between the three detectors' noises, as well as between the noises and the signal, are negligible; thus, we can write the residual as

$$R = \frac{1}{1 + \frac{1}{SNR_L^2 + SNR_H^2 + SNR_V^2}}, \tag{13}$$

where $SNR_i^2 = E[x,x]/E[n_i,n_i]$ is the signal-to-noise ratio (SNR) of each detector i. Thus, using more detectors helps to enhance the total SNR and improves the residual. Having a detector with a much smaller SNR does not decrease the capability of the Wiener filter; however, it does not contribute much to lowering the residual relative to the other two detectors. Of course, any correlation between the signal and the detector's noise and between different detectors can spoil the residual.

IV. RESULTS

The Wiener filter requires a model for the target signal to perform the cross-PSD between it and the witness signals. Since the target signal is usually immersed in noise, and we cannot disentangle the two, we must use templates for the ultralight dark-matter target signal. We injected templates of vector ultralight dark-matter signals (dark photons) in the data with different frequencies. Indeed, when we search for a signal in the data, we do not know which frequency or amplitude it could have. We only know it is almost monochromatic, and we can model it for different frequencies. We can therefore search for the right signal by calculating the residual [Eq. (12)] for many templates with

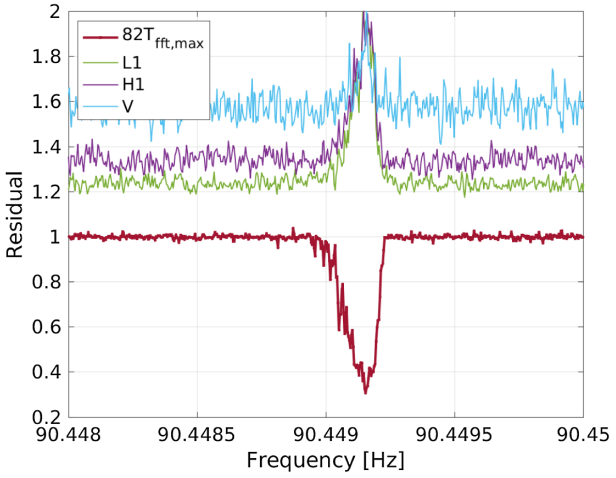

FIG. 1. Comparison between the shape of the residual and the three detectors' PSDs for an injected dark photon dark-matter signal. Each detector's PSD has been normalized and vertically shifted by 1 to easily compare it with the residual shape. In this plot, $\epsilon = 10^{-22}$.

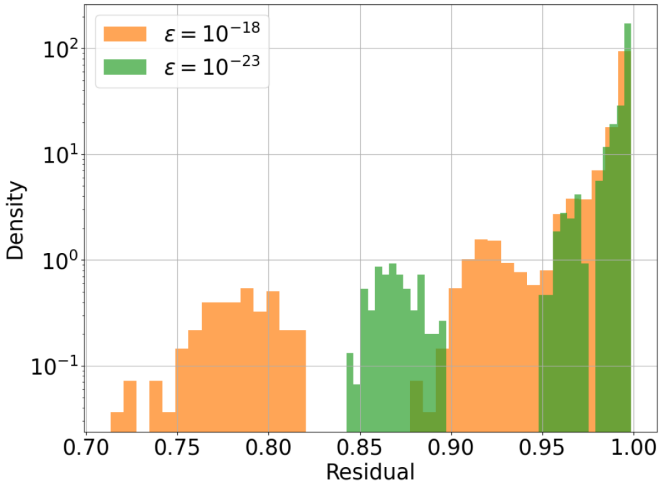

FIG. 2. This plot provides a background distribution for the residual, to which we can compare the residuals from interesting dark-matter candidates obtained in a real search. These residuals are calculated using 3861 dark-photon templates with frequencies between 40 and 1990 Hz that differed from the injected one ($f_0 = 90.449$ Hz, $m_A = 3.741 \times 10^{-13}$ eV/c^2). The mean and standard deviation of this residual distribution are 0.98 and 0.037 and 0.99 and 0.021 for the injected signal with $\epsilon = 10^{-18}$ and $\epsilon = 10^{-23}$, respectively.

different frequencies. The template should be, in principle, multiplied by ϵ_t, the coupling value of the target template, to simulate different amplitudes, but we can see from Eq. (12) that the value of ϵ_t does not affect the residual, since it is contained in $X(\omega)$ and thus cancels out. For our purposes, then, we do not need to consider ϵ_t as a parameter for ultralight dark-matter searches with the Wiener filter. Instead, the signal strength, ϵ, will affect the residual, since it is contained in the measured $Y(\omega)$ signal and will change the SNR (see Sec. III B). In Fig. 1, we show that the residual width and shape coincide with the PSD signal width. By injecting signals with different ϵ, we can see that the minimum residual value decreases with ϵ; thus, the SNR will increase.

A. Detection statistic

We would like to employ the Wiener filter as a validation method for the search of ultralight dark-matter signals. In this respect, our target signal will be the modeled ultralight dark-matter signal, while the witness sensors will be the gravitational-wave detectors. Equation (12) provides an estimation for whether the target signal is present in the data; the lower the residual, the more likely it is that the target signal and data match. To distinguish potential ultralight dark-matter candidates from detector noise, we should employ the residual as a detection statistic. While we have so far understood that low residuals imply the presence of the target signal, we have not yet discussed how to quantify a "low enough" residual to claim that signal as "significant." To do this, we must construct a background distribution for the residual; i.e., what residuals would we obtain if the target signal and that in the data were not a match? Once we have this distribution, we can place a threshold, $R_{\rm thr}$, below which we would consider a signal as interesting.

In practice, we injected 39 ultralight dark-matter signals into the LIGO Hanford, LIGO Livingston, and Virgo detectors' data streams from the third observing run (O3). For each one of these data streams, we evaluated 99 residuals using a target signal with a different frequency. Hence, we have 3861 templates with which to construct our background distribution for the Wiener filter residual. Figure 2 shows the histogram of all the residuals obtained, in two cases: 1) the signal we injected is strong ($\epsilon = 10^{-18}$) and 2) the signal is very weak ($\epsilon = 10^{-23}$). We can see that in both cases residuals do not go below 0.70, meaning that in a real search $R_{\rm thr} < 0.7$, depending on what level of significance we wish to use to claim a candidate is interesting. If a template returns a value for the residual above $R_{\rm thr}$, we can veto the outlier at that particular frequency; if it returns a residual value lower than $R_{\rm thr}$, it warrants further investigation. When we apply the Wiener filter to outliers in O3 [23], as described in Sec. IV C, we take $R_{\rm thr} = 0.7$.

B. Application of Wiener filter

To apply the Wiener filter in the context of ultralight dark-matter searches in data from gravitational-wave interferometers, we should understand what residuals to expect as a function of the strength of a potential dark-matter signal. In a real search, we would then be able to map our residuals to strain amplitude of a signal and, in the case of

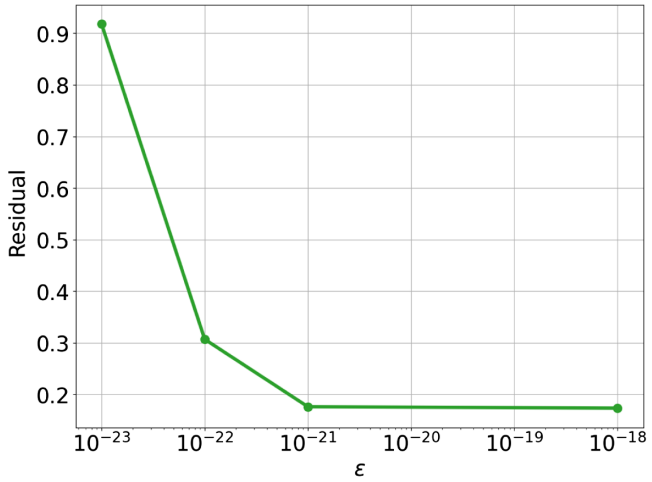

FIG. 3. Value of the minimum residual (corresponding to the frequency of the dark photon signal) vs the coupling strengths used to generate a dark photon signal with $T_{\mathrm{FFT}} = 82T_{\mathrm{FFT,max}}$. The injected signal frequency is $f_0 = 90.449$ Hz ($m_A = 3.741 \times 10^{-13}$ eV/c^2).

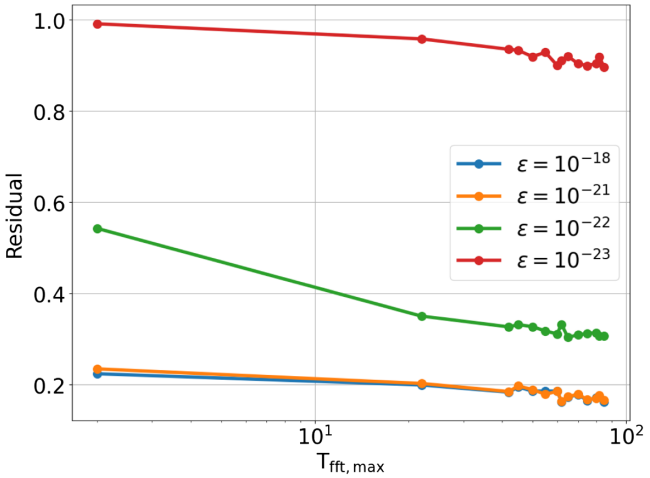

FIG. 4. Residuals vs the length of the fast Fourier transform, in terms of the maximum allowed fast Fourier transform $T_{\mathrm{FFT,max}}$, for injected dark photon signals with different coupling strengths. We see that for very strong (orange, blue) and very weak signals (red) the reduction in the residuals with increasing T_{FFT} is marginal compared to an intermediate-strength signal (green). The injected signal frequency is $f_0 = 90.449$ Hz ($m_A = 3.741 \times 10^{-13}$ eV/c^2).

dark photons, the coupling ϵ. We inject the same signal with various coupling strengths into O3 Hanford, Livingston, and Virgo data and apply the Wiener filter to obtain residuals. We plot the residual value at the frequency of the dark-matter signal in Fig. 3 as a function of ϵ. This plot gives an indication of the sensitivity of the Wiener filter method to extract weak dark-matter signals from the data, though a full sensitivity study is beyond the scope of this work.

We apply the frequency domain Wiener filter on data that have been Fourier transformed, and the length of each fast Fourier transform may impact the residual values we obtain. This is because as we increase T_{FFT} beyond $T_{\mathrm{FFT,max}} \sim v_0^2/c^2 f \sim 10^{-6} f$ Hz, the maximum allowed fast Fourier transform that would confine frequency modulations to one frequency bin, we start to observe more and more power spreading in the frequency domain near the signal frequency. Thus, in Fig. 4, we determine, for different dark photon coupling strengths, the values of the residual as a function of increasing T_{FFT}. Increasing T_{FFT} appears to decrease the value of the minimum residual, thus helping to better distinguish the ultralight dark-matter signal from noise, which is especially true in the "intermediate" signal strength regime, i.e., $\epsilon = 10^{-22}$. Eventually, however, the residual value tends to saturate around $T_{\mathrm{FFT}} = 40T_{\mathrm{FFT,max}}$, implying that we would not improve our estimation of the residual in a real search with $T_{\mathrm{FFT}} > 40T_{\mathrm{FFT,max}}$.

We can understand why this saturation of the residuals at a particular T_{FFT} happens by looking at Fig. 5. Here, we show how the residual shape changes with different fast Fourier transform lengths for the green curve ($\epsilon = 10^{-22}$) in Fig. 4. We observe very little difference in the residuals between curves with $T_{\mathrm{FFT}} \geq 22T_{\mathrm{FFT,max}}$ because the power spreading that occurs beyond $22T_{\mathrm{FFT,max}}$ does not result in significant SNR loss.

C. Follow-up of candidates to rule out noise disturbances

The search for dark photon dark matter in LIGO/Virgo O3 data [23] using an excess power method [36] returned 11 coincident outliers (i.e., particular frequencies) with critical ratios (our detection statistic) greater than 5,

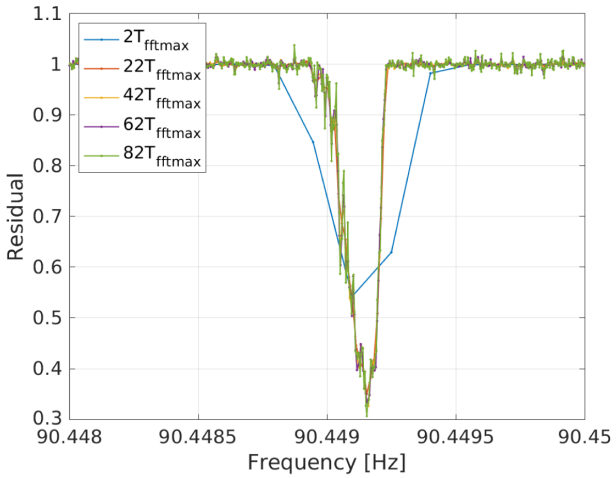

FIG. 5. Comparison between different fast Fourier transform lengths applied to an injected dark photon dark-matter signal. When increasing T_{FFT}, the residual width around the dark photon signals tends to stabilize around that of the PSD (see Fig. 1). In this plot, $\epsilon = 10^{-22}$.

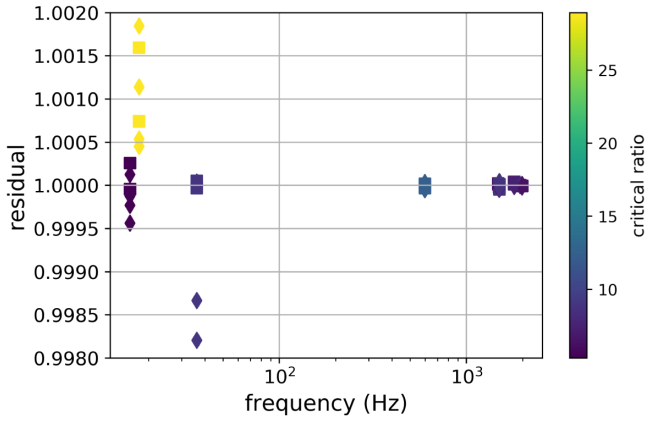

FIG. 6. Residuals for each of the 11 outliers as a function of frequency, with the critical ratio (detection statistic in the excess power search in Ref. [23]) colored, obtained using both scalar and dark photon dark-matter models. Squares indicate residuals calculated using a pair of detectors (HL, LV, or HV), while diamonds denote residuals calculated for a single detector. Even for high values of the critical ratio, the residual values are very close to 1, showing that the Wiener filter can successfully veto outliers that appear in the initial analysis [23,36]. We use $T_{\mathrm{FFT}} = 2T_{\mathrm{FFT,max}}$ here at each frequency.

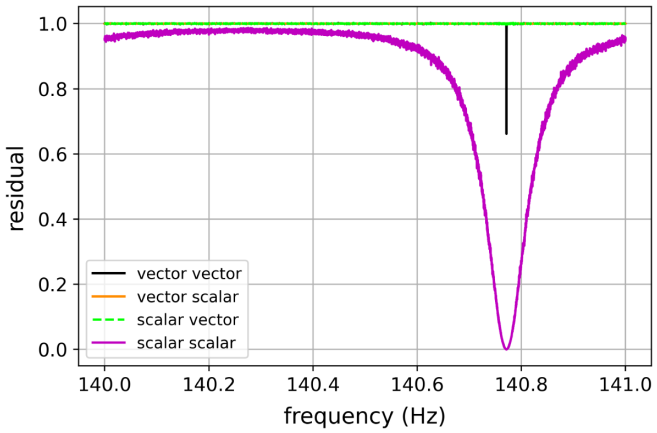

FIG. 7. Residuals obtained for an injection with $f_0 = 140.77$ Hz ($m_\phi = m_A = 5.82 \times 10^{-13}$ eV$/c^2$) and a strain amplitude of 10^{-22} and 10^{-24} for the scalar and vector injected signals, respectively. The residuals of filtering a scalar injection with a vector model, and vice versa, are so close to 1 and are indistinguishable. Here, $T_{\mathrm{FFT}} = 2T_{\mathrm{FFT,max}}$.

implying that there could have been a signal at these frequencies. At the time, these outliers were vetoed by manually studying the spectra created with different fast Fourier transform lengths and showing that the outliers were, in fact, coincident with various noise disturbances in the data that became apparent at different fast Fourier transform lengths. Instead of studying by eye each of the spectra, we can use the Wiener filter to veto these outliers, by showing that their residuals are approximately equal to 1, which is what is expected when the target waveform (i.e., the dark photon or scalar dark-matter signal) does not match the waveform returned by the analysis method.

Figure 6 shows the values of the residuals for each of the 11 outliers in the O3 analysis returned by the excess-power method (Table II in Ref. [23]), for the cases of applying the Wiener filter, with models of both a scalar and dark photon dark-matter signal, to the data of each detector separately (diamonds) and then jointly (squares) for Hanford-Livingston (HL), Livingston-Virgo (LV), and Hanford-Virgo (HV). The color represents the values of the critical ratio returned by the original O3 search. Despite having high critical ratios, the values of the residuals for each of these outliers are nearly 1, underscoring the effectiveness of the Wiener filter in vetoing such outliers even when the detection statistic takes a high value, i.e., greater than 5, our threshold in the analysis.

D. Ability to distinguish between dark-matter interactions

Because the Wiener filter requires a specific model, we can use it as a way to identify exactly what kind of dark-matter signal is present in the data. In contrast to its deterministic counterpart, the matched filter, it should return a small value of the residual when the signal model matches what is present in the data and a large value when the wrong model is used. To test this claim, we simulate both scalar and vector dark-matter interaction signals and inject them into real LIGO O2 Livingston data within the Band Sampled Data framework [69]. We then filter the data with a scalar injection, simulated based on codes available from Ref. [21], with a model for a vector signal that arises from an ultralight dark-matter particle with the same mass, and vice versa, to determine whether the Wiener filter will fail. For comparison, we also filter the data containing scalar and vector injections with themselves, to obtain the optimal, low value of the residual.

We show the frequency spectrum for injected scalar and vector dark-matter signals when applying both scalar and vector signal filters in Fig. 7. Here, we see that the residuals obtained when filtering with the wrong model at the right frequency are $\sim$1, while filtering with the correct signal gives values less than 1. We note here that the injected vector (dark photon) dark-matter signals are not that strong ($\epsilon = 10^{-22}$), which explains the residual values around $\sim$0.7. If we had injected the same or a stronger signal in O3 data, we would have obtained lower residuals, similar to those shown in Fig. 3.

We now expand our analysis to a sample of randomly chosen injections. In Fig. 8(a), we plot the residual as a function of injected signal frequency for ten injections. Here, we see that scalar injections filtered by vector models, and vice versa, give values of the residual close to 1, while filtering the data with the exact model of the signal injected gives residual values that are more indicative of a signal (based on Fig. 2).

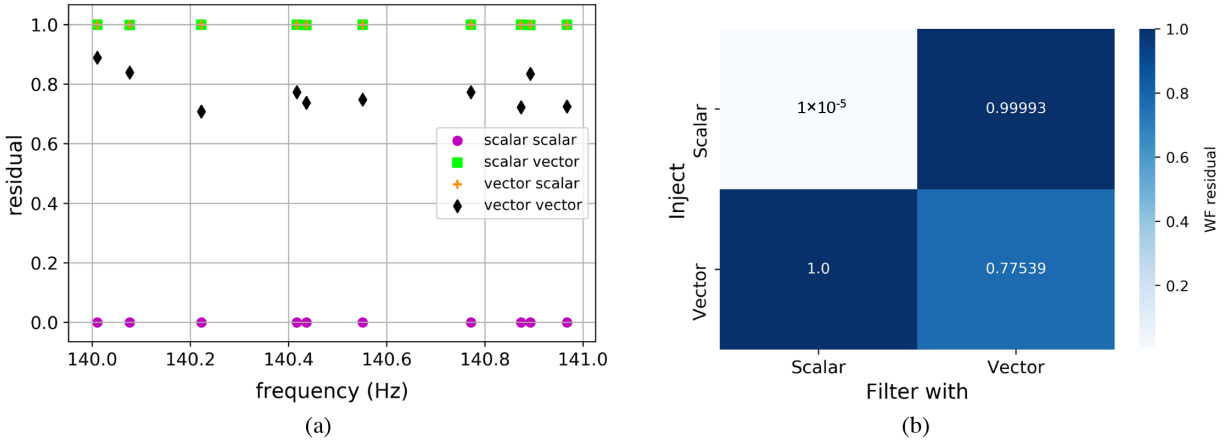

FIG. 8. Left: residuals obtained from filtering ten injected scalar or vector dark-matter signals with scalar or vector waveforms. The strain amplitude of the scalar and vector signals are $\sim 10^{-22}$ and $\sim 10^{-25}$ ($\epsilon = 10^{-22}$), respectively, which explains why the residuals for the "scalar filtered with scalar" case are so much lower than the "vector filtered with vector" case. Right: average of residuals obtained from filtering ten scalar and vector injections with scalar and vector models. Lower values of the residuals imply that, on average, the injected signal is well recovered, while residuals close to unity indicate that the injected signal is not found. We have employed $T_{\mathrm{FFT}} = 2T_{\mathrm{FFT,max}}$ here.

We also plot, in Fig. 8(b), a "confusion matrix" for the four permutations of injecting and filtering with scalar and vector signals. The numbers shown here are the average residuals across ten scalar or vector injections when filtering with either the scalar or vector waveforms. Figure 8(b) illustrates conceptually the ability of the Wiener filter to distinguish between different dark-matter models.

V. CONCLUSIONS

In this paper, we have shown that the Wiener filter can recover scalar and vector dark matter that interact directly with gravitational-wave interferometers. Within the context of method development, we have derived a detection statistic that can be used in a real search to quantify whether a dark-matter signal is present in the data. We have shown what residuals to expect for various dark photon dark matter coupling strengths and have computed how the residuals would improve with increasing fast Fourier transform length. We have also determined that the Wiener filter can be employed as a robust follow-up method in ultralight dark-matter searches, which confirm or deny the presence of outliers with high detection statistic values. Finally, we have shown that the Wiener filter can distinguish between different dark-matter signal models.

Our work represents the first step toward the inclusion of a robust follow-up method to determine the existence of ultralight dark matter and provides a proof-of-concept study on the efficiency of the Wiener filter in ultralight dark-matter searches. Future work will include performing a comprehensive sensitivity study for various ultralight dark-matter signals with different amplitudes and using different fast Fourier transform lengths, the development of a generic "template" based solely on the Maxwell-Boltzmann velocity distribution that could enhance the signal in a model-independent way before the application of the Wiener filter, an estimate of the computational cost to employ the Wiener filter as a complete method for ultralight dark-matter searches, and a comparison with standard techniques already employed to detect ultralight dark matter. We will also expand the Wiener filter to search for tensor dark matter [70], which could arise from modifications to gravity, e.g., bimetric gravity [71,72], due to an additional spin-2 particle that would act as dark matter. It has already been shown that current and future detectors, such as Cosmic Explorer [73] and Einstein Telescope [74] on the ground and DECIGO [75], LISA [76], and TianQin [77] in space, could also be sensitive to tensor dark matter [78] and, in general, greatly lower the noise floor, enhance our sensitivity to these types of dark-matter interaction signals, and cover an even lighter range of dark-matter masses, i.e., $\mathcal{O}(10^{-17}$–$10^{-15})$ eV$/c^2$. The future is bright for Wiener filter–based methods to not only follow-up candidates of other searches but also to directly search for ultralight dark-matter interactions on Earth and in space.

ACKNOWLEDGMENTS

This material is based upon work supported by NSF's LIGO Laboratory, which is a major facility fully funded by the National Science Foundation. We thank Ornella J. Piccinni, and Sergio Frasca for the development of the Band Sampled Data framework that allowed us to easily perform simulations of dark-matter signals. We also are grateful to Cristiano Palomba for the idea to use the Wiener filter to extract the (stochastic) dark-matter signal from the

noise, and distinguish between models. We thank Bernard Whiting for additional discussions regarding matched filtering and the physics of the dark photon dark-matter signal, and the Amaldi Research Centre at Sapienza Università di Roma for support. We thank the anonymous referee for their comments on the manuscript, which have significantly improved the paper. This research has made use of data, software and/or web tools obtained from the Gravitational Wave Open Science Center [79], a service of LIGO Laboratory, the LIGO Scientific Collaboration, and the Virgo Collaboration. LIGO Laboratory and Advanced LIGO are funded by the United States National Science Foundation (NSF) as well as the Science and Technology Facilities Council (STFC) of the United Kingdom, the Max-Planck-Society (MPS), and the State of Niedersachsen/Germany. This funding supports the construction of Advanced LIGO and construction and operation of the GEO600 detector. Additional support for Advanced LIGO was provided by the Australian Research Council. Virgo is funded, through the European Gravitational Observatory (EGO), by the French Centre National de Recherche Scientifique (CNRS), the Italian Istituto Nazionale della Fisica Nucleare (INFN), and the Dutch Nikhef, with contributions by institutions from Belgium, Germany, Greece, Hungary, Ireland, Japan, Monaco, Poland, Portugal, and Spain. Computational resources have been provided by the supercomputing facilities of the Université catholique de Louvain (CISM/UCL) and the Consortium des Équipements de Calcul Intensif en Fédération Wallonie Bruxelles (CÉCI) funded by the Fond de la Recherche Scientifique de Belgique (F.R.S.-FNRS) under convention 2.5020.11 and by the Walloon Region. We also wish to acknowledge the support of the INFN-CNAF computing center for its help with the storage and transfer of the data used in this paper. The authors gratefully acknowledge the support of the NSF, STFC, INFN, and CNRS for provision of computational resources. All plots were made with the PYTHON tools MATPLOTLIB, NUMPY, and PANDAS. A. L. M. is a beneficiary of a FSR Incoming Post-doctoral Fellowship.

[1] E. Corbelli and P. Salucci, Mon. Not. R. Astron. Soc. **311**, 441 (2000).
[2] D. Clowe, A. Gonzalez, and M. Markevitch, Astrophys. J. **604**, 596 (2004).
[3] N. Sugiyama, Astrophys. J. Suppl. Ser. **100**, 281 (1995).
[4] J. L. Feng, Annu. Rev. Astron. Astrophys. **48**, 495 (2010).
[5] A. M. Green and B. J. Kavanagh, J. Phys. G **48**, 043001 (2021).
[6] E. Aprile *et al.* (XENON Collaboration), Phys. Rev. D **94**, 092001 (2016); **95**, 059901(E) (2017).
[7] R. Agnese *et al.* (SuperCDMS Collaboration), Phys. Rev. Lett. **121**, 051301 (2018); **122**, 069901(E) (2019).
[8] P. Agnes *et al.* (DarkSide Collaboration), Phys. Rev. Lett. **121**, 111303 (2018).
[9] J. M. Gaskins, Contemp. Phys. **57**, 496 (2016).
[10] J. Aasi, B. P. Abbott, R. Abbott, T. Abbott, M. R. Abernathy, K. Ackley, C. Adams, T. Adams, P. Addesso *et al.*, Classical Quantum Gravity **32**, 115012 (2015).
[11] F. Acernese, M. Agathos, K. Agatsuma, D. Aisa, N. Allemandou, A. Allocca, J. Amarni, P. Astone, G. Balestri, G. Ballardin *et al.*, Classical Quantum Gravity **32**, 024001 (2015).
[12] Y. Aso, Y. Michimura, K. Somiya, M. Ando, O. Miyakawa, T. Sekiguchi, D. Tatsumi, and H. Yamamoto (KAGRA Collaboration), Phys. Rev. D **88**, 043007 (2013).
[13] M. Maggiore, *Gravitational Waves: Volume 1: Theory and Experiments* (Oxford University Press, Oxford, 2008), Vol. 1.
[14] K. L. Dooley *et al.*, Classical Quantum Gravity **33**, 075009 (2016).
[15] M. Tröbs and G. Heinzel, Measurement **39**, 120 (2006).
[16] M. Tröbs and G. Heinzel, Measurement **42**, 170 (2009).
[17] Y. Stadnik and V. Flambaum, Phys. Rev. Lett. **114**, 161301 (2015).
[18] Y. Stadnik and V. Flambaum, Phys. Rev. Lett. **115**, 201301 (2015).
[19] Y. Stadnik and V. Flambaum, Phys. Rev. A **93**, 063630 (2016).
[20] H. Grote and Y. Stadnik, Phys. Rev. Research **1**, 033187 (2019).
[21] S. M. Vermeulen *et al.*, Nature (London) **600**, 424 (2021).
[22] H.-K. Guo, K. Riles, F.-W. Yang, and Y. Zhao, Commun. Phys. **2**, 1 (2019).
[23] R. Abbott *et al.* (LIGO Scientific, Virgo, KAGRA Collaborations), Phys. Rev. D **105**, 063030 (2022).
[24] S. Schlamminger, K. Y. Choi, T. A. Wagner, J. H. Gundlach, and E. G. Adelberger, Phys. Rev. Lett. **100**, 041101 (2008).
[25] J. Bergé, P. Brax, G. Métris, M. Pernot-Borràs, P. Touboul, and J.-P. Uzan, Phys. Rev. Lett. **120**, 141101 (2018).
[26] C. Palomba, S. D'Antonio, P. Astone, S. Frasca, G. Intini, I. La Rosa, P. Leaci, S. Mastrogiovanni, A. L. Miller, F. Muciaccia *et al.*, Phys. Rev. Lett. **123**, 171101 (2019).
[27] L. Sun, R. Brito, and M. Isi, Phys. Rev. D **101**, 063020 (2020); **102**, 089902(E) (2020).
[28] M. Isi, L. Sun, R. Brito, and A. Melatos, Phys. Rev. D **99**, 084042 (2019).
[29] S. D'Antonio, C. Palomba, P. Astone, S. Frasca, G. Intini, I. La Rosa, P. Leaci, S. Mastrogiovanni, A. Miller, F. Muciaccia *et al.*, Phys. Rev. D **98**, 103017 (2018).
[30] K. K. Y. Ng, S. Vitale, O. A. Hannuksela, and T. G. F. Li, Phys. Rev. Lett. **126**, 151102 (2021).

[31] S. J. Zhu, M. Baryakhtar, M. A. Papa, D. Tsuna, N. Kawanaka, and H.-B. Eggenstein, Phys. Rev. D **102**, 063020 (2020).
[32] L. Tsukada, T. Callister, A. Matas, and P. Meyers, Phys. Rev. D **99**, 103015 (2019).
[33] R. Abbott *et al.* (LIGO Scientific, Virgo Collaborations), Phys. Rev. Lett. **125**, 101102 (2020).
[34] J. C. Bustillo, N. Sanchis-Gual, A. Torres-Forné, J. A. Font, A. Vajpeyi, R. Smith, C. Herdeiro, E. Radu, and S. H. W. Leong, Phys. Rev. Lett. **126**, 081101 (2021).
[35] A. Pierce, K. Riles, and Y. Zhao, Phys. Rev. Lett. **121**, 061102 (2018).
[36] A. L. Miller *et al.*, Phys. Rev. D **103**, 103002 (2021).
[37] N. Wiener *et al.*, *Extrapolation, Interpolation, and Smoothing of Stationary Time Series: With Engineering Applications* (MIT Press, Cambridge, MA, 1964), Vol. 8.
[38] D. Carney, A. Hook, Z. Liu, J. M. Taylor, and Y. Zhao, New J. Phys. **23**, 023041 (2021).
[39] R. D. Peccei and H. R. Quinn, Phys. Rev. Lett. **38**, 1440 (1977).
[40] R. D. Peccei and H. R. Quinn, Phys. Rev. D **16**, 1791 (1977).
[41] S. Weinberg, Phys. Rev. Lett. **40**, 223 (1978).
[42] F. Wilczek, Phys. Rev. Lett. **40**, 279 (1978).
[43] J. Preskill, M. B. Wise, and F. Wilczek, Phys. Lett. **120B**, 127 (1983).
[44] L. Abbott and P. Sikivie, Phys. Lett. **120B**, 133 (1983).
[45] M. Dine and W. Fischler, Phys. Lett. **120B**, 137 (1983).
[46] Y. Cho and Y. Keum, Mod. Phys. Lett. A **13**, 109 (1998).
[47] Y. Cho and J. Kim, Phys. Rev. D **79**, 023504 (2009).
[48] A. Arvanitaki, J. Huang, and K. Van Tilburg, Phys. Rev. D **91**, 015015 (2015).
[49] K. Nagano, T. Fujita, Y. Michimura, and I. Obata, Phys. Rev. Lett. **123**, 111301 (2019).
[50] K. Nagano, H. Nakatsuka, S. Morisaki, T. Fujita, Y. Michimura, and I. Obata, Phys. Rev. D **104**, 062008 (2021).
[51] A. Derevianko, Phys. Rev. A **97**, 042506 (2018).
[52] A. E. Nelson and J. Scholtz, Phys. Rev. D **84**, 103501 (2011).
[53] P. Arias, D. Cadamuro, M. Goodsell, J. Jaeckel, J. Redondo, and A. Ringwald, J. Cosmol. Astropart. Phys. 06 (2012) 013.
[54] P. W. Graham, J. Mardon, and S. Rajendran, Phys. Rev. D **93**, 103520 (2016).
[55] P. Agrawal, N. Kitajima, M. Reece, T. Sekiguchi, and F. Takahashi, Phys. Lett. B **801**, 135136 (2020).
[56] R. T. Co, A. Pierce, Z. Zhang, and Y. Zhao, Phys. Rev. D **99**, 075002 (2019).
[57] M. Bastero-Gil, J. Santiago, L. Ubaldi, and R. Vega-Morales, J. Cosmol. Astropart. Phys. 04 (2019) 015.
[58] J. A. Dror, K. Harigaya, and V. Narayan, Phys. Rev. D **99**, 035036 (2019).
[59] A. J. Long and L.-T. Wang, Phys. Rev. D **99**, 063529 (2019).
[60] Y. Michimura, T. Fujita, S. Morisaki, H. Nakatsuka, and I. Obata, Phys. Rev. D **102**, 102001 (2020).
[61] S. Morisaki, T. Fujita, Y. Michimura, H. Nakatsuka, and I. Obata, Phys. Rev. D **103**, L051702 (2021).
[62] F. Badaracco *et al.*, Classical Quantum Gravity **37**, 195016 (2020).
[63] P. M. Meyers, K. Martinovic, N. Christensen, and M. Sakellariadou, Phys. Rev. D **102**, 102005 (2020).
[64] E. Thrane, N. Christensen, R. M. S. Schofield, and A. Effler, Phys. Rev. D **90**, 023013 (2014).
[65] M. W. Coughlin *et al.*, Classical Quantum Gravity **33**, 224003 (2016).
[66] M. W. Coughlin *et al.*, Phys. Rev. D **97**, 102007 (2018).
[67] S. V. Vaseghi, Wiener filters, in *Advanced Digital Signal Processing and Noise Reduction* (Wiley, New York, 2001), pp. 178–204.
[68] J. O. Smith, *Introduction to Digital Filters: With Audio Applications* (W3K Publishing, USA, 2007), Vol. 2.
[69] O. Piccinni, P. Astone, S. D'Antonio, S. Frasca, G. Intini, P. Leaci, S. Mastrogiovanni, A. Miller, C. Palomba, and A. Singhal, Classical Quantum Gravity **36**, 015008 (2019).
[70] L. Marzola, M. Raidal, and F. R. Urban, Phys. Rev. D **97**, 024010 (2018).
[71] S. F. Hassan and R. A. Rosen, J. High Energy Phys. 02 (2012) 126.
[72] A. Schmidt-May and M. von Strauss, J. Phys. A **49**, 183001 (2016).
[73] D. Reitze *et al.*, Bull. Am. Astron. Soc. **51**, 035 (2019).
[74] M. Punturo, M. Abernathy, F. Acernese, B. Allen, N. Andersson, K. Arun, F. Barone, B. Barr, M. Barsuglia, M. Beker *et al.*, Classical Quantum Gravity **27**, 194002 (2010).
[75] S. Kawamura *et al.*, Prog. Theor. Exp. Phys. **2021**, 05A105 (2021).
[76] S. Babak, J. Gair, A. Sesana, E. Barausse, C. F. Sopuerta, C. P. L. Berry, E. Berti, P. Amaro-Seoane, A. Petiteau, and A. Klein, Phys. Rev. D **95**, 103012 (2017).
[77] J. Luo *et al.* (TianQin Collaboration), Classical Quantum Gravity **33**, 035010 (2016).
[78] J. M. Armaleo, D. L. Nacir, and F. R. Urban, J. Cosmol. Astropart. Phys. 04 (2021) 053.
[79] https://www.gw-openscience.org/.